THREE-DIMENSIONAL NON-LINEAR FINITE ELEMENT ANALYSIS OF IMPACT RESPONSE AND DAMAGE IN LAMINATED COMPOSITE SHELLS

Surendra Kumar*

Abstract

The impact response and the impact-induced damage in curved composite laminates subjected to transverse impact by a metallic impactor are studied using three-dimensional non-linear transient dynamic finite element formulation. A layered version of isoparametric eight-noded hexahedral element with incompatible modes is developed which incorporates geometrical non-linearity based on total Langragian approach. The non-linearity of both strain displacement relation and contact loading are simultaneously solved using Newton-Raphson incrementaliterative method. Impact-induced damages (matrix cracking and delamination) are predicted using appropriate three-dimensional stress-based failure criteria. Some example problems of graphite/epoxy laminated cylindrical shells with variation of important parameters such as impactor velocity, shell curvature, laminate dimension and fibre orientation of plies are solved and the influence of geometrical non-linear effect on both impact response and resulting damages is demonstrated.

***Keywords**: Finite element analysis, geometrical non-linearity, 8-noded layered brick element, polymer matrix composites, curved laminates, impact dynamics.*

Introduction

Resistance of the damage caused by low velocity non-penetrating impact is an important design consideration in case of fibre-reinforced plastic laminated composite structure. Therefore, numerous experimental and analytical investigations have been performed for understanding impact response and impact-induced damages in these laminates; the summary of most of the earlier work is reported in References [1-2].

A number of researchers have deployed the 2-D and 3-D finite element method for the solution of impact problems for laminated plates and shells. Earlier numerical investigations were mainly based on small deflection theory and didn't consider non-linear effects [3-7]. Ambur et al. [8] have concluded that the inclusion of geometrical non-linearity in the prediction of impact response and damage in thin and moderately thick laminated composites helps in improving the accuracy of the analysis. Chandrashekhara and Schroeder [9] have studied impact response of laminated curved shell using finite element formulation based on Sander's shell theory considering geometric non-linearity in the sense of von Karman strains. However, impact damage was not investigated in their study. Kam et al. [10] predicted deflection and first ply failure load of thin laminated composite plates using a non-linear finite element model based on Mindlin plate theory. The prediction of ultimate strength of the damaged plate was based on the hypothetical strength reduction model that once a matrix crack is predicted at a point, it is assumed to be extended through the full width of the plate. Ganapathy and Rao [11] used 4-noded 48 d.o.f shell element based on Kirchhoff-Love thin shell theory in non-linear finite element analysis of cylindrical/spherical shell panels. The authors used a form of classical Hertzian contact law and predicted matrix cracking failure by applying the general Tsai-Wu failure criterion for composite materials. Although geometrical non-linearity was included, the study assumes that low velocity impact force and deformation can be simulated by static model and hence does not compute impact response as a function of time. Krishnamurthy et. al. [12] used 9 noded isoparametric shell element based on Mindlin-Reissener assumptions regarding transverse shear deformations in their parametric study of laminated cylindrical shell and assumed parabolic shear stress distribution across the thick-

* CSIR Centre for Mathematical Modelling and Computer Simulation (CMMACS), Council of Scientific and Industrial Research (CSIR), National Aerospace Laboratories, Belur Campus, Wind Tunnel Road, Bangalore-560 037, India
Email : surendra@cmmacs.ernet.in
Manuscript received on 08 Jun 2009; Paper reviewed, revised and accepted as a Full Length Contributed Paper on 04 Jan 2010

ness. Zhu et al. [13] incorporated effects of strain rate dependency and inelastic behavior of matrix material for analyzing the mechanical response of laminated shell. The study was, however, concentrated on transient response of laminated shell subjected to suddenly applied static loading uniformly distributed over the bottom surface of the panel and didnt consider damage phenomena. More recently, Kumar [14] has carried out non-linear finite element transient dynamic analysis to predict impact response and impact-induced damage in laminated composite cylindrical shell using eight-noded isoparametric quadrilateral shell element. The shell element used was based on Sander's shell theory [15] and incorporated geometrical nonlinearity as given by Stein [16].

The present paper is aimed towards understanding non-linear effects on impact behavior and resulting damage in curved composite laminate subjected to transverse impact by a metallic impactor using a three-dimensional non-linear transient dynamic finite element formulation. A layered version of isoparametric eight noded hexahedral element with incompatible modes is developed. Geometrical non-linearity is incorporated based on total Lagrangian approach and the generalized Greens strain tensor is used in the strain-displacement relationships. The non-linear system of equations resulting from large displacement formulation and non-linear contact law are simultaneously solved using modified Newton-Raphson incremental-iterative method. Example problems of graphite/epoxy cylindrically curved shell are studied with parametric variations and the influence of geometrical non-linearity on the impact response and impact-induced damage is investigated.

Finite Element Methodology

Governing Equations

Finite element dynamic equilibrium equation is derived using the Hamilton's principle. It states that the variation of the energy functional during any time interval t_1 to t_2 must be equal to zero, i.e.

$$\delta \int_{t_1}^{t_2} \Pi \, dt = \int_{t_1}^{t_2} (\delta T - \delta U + \delta W) \, dt = 0 \qquad (1)$$

The variations in strain energy U, the work done on the structure by external loads W and the kinetic energy T are defined as:

$$\delta U = \int_V \{\delta \varepsilon\}^T \{\sigma\} \, dV,$$

$$\delta W = \int_V \{\delta u\}^T \{b\} \, dV + \int_S \{\delta u^s\}^T \{p\} \, dS + \sum_i \{\delta u^i\}^T \{f_c^i\}$$

and

$$\delta T = \int_V \rho \{\delta \dot{u}\}^T \{\dot{u}\} \, dV. \qquad (2)$$

where V and S represent volume and surface of the body. ρ is the mass density of the material. $\{b\}$ is the body force vector at any point in the continuum and $\{p\}$ is the surface force vector at any point on the surface of the body. The superscript s denotes that surface displacements are considered and the superscript i denotes the displacements at the point where the concentrated forces $\{f_c^i\}$ are applied. $\{\delta u\}$ and $\{\delta \varepsilon\}$are vectors of virtual displacement and virtual strains respectively. $\{\sigma\}$ is the stress vector at any point.

Now, integration of the δT term by parts with respect to time gives:

$$\int_{t_1}^{t_2} \int_V \rho \{\delta \dot{u}\}^T \{\dot{u}\} \, dV \, dt = \int_V \rho \left[\{\delta \dot{u}\}^T \{\dot{u}\} \right]_{t_1}^{t_2} dV$$

$$- \int_{t_1}^{t_2} \int_V \rho \{\delta u\}^T \{\ddot{u}\} \, dV \, dt. \qquad (3)$$

According to Hamilton's principle, the displacement configuration must satisfy the conditions given at time t_1 and t_2. Hence, $\{\delta u(t_1)\} = \{\delta u(t_2)\} = \{0\}$ and the first term of right hand side of Eq. (3) vanishes.

Substitution of Eq. (2) along with second right hand side term of Eq. (3) into Eq. (1) and rearranging, we get

$$\int_V \{\delta \varepsilon\}^T \{\sigma\} \, dV + \int_V \rho \{\delta u\}^T \{\ddot{u}\} \, dV - \int_V \{\delta u\}^T \{b\} \, dV$$

$$- \int_S \{\delta u^s\}^T \{p\} \, dS - \sum_i \{\delta u^i\}^T \{f_c^i\} = 0 \qquad (4)$$

Eq. (4) can now be rewritten as a sum of integration over the volume and areas of all finite elements, i.e.

$$\sum_e \int_{V_e} \{\delta \varepsilon\}^T \{\sigma\} \, dV + \sum_e \int_{V_e} \rho \{\delta u\}^T \{\ddot{u}\} \, dV - \sum_e \int_{V_e} \{\delta u\}^T \{b\} \, dV$$

$$- \sum_e \int_{S_e} \{\delta u^s\}^T \{p\} \, dS - \sum_i \{\delta u^i\}^T \{f_c^i\} = 0 \qquad (5)$$

The displacements and accelerations within each element *e* are related to the nodal displacements by its shape function matrix [*N*] so that:

$$\{u\} = [N]\{U\} \quad \text{and}$$

$$\{\ddot{u}\} = [N]\{\ddot{U}\}. \tag{6}$$

In large displacement problem, strains within each element *e* are related to the nodal displacements as

$$\{\varepsilon\} = [\bar{B}]\{U\} = \left[[B_L] + \frac{1}{2}[B_{NL}]\right]\{U\}, \tag{7}$$

where $[\bar{B}]$ is strain-displacement matrix, $[B_L]$ is the contribution from the linear part of the Green's strain and $\frac{1}{2}[B_{NL}]$ is the contribution from the quadratic part of the Green's strain. $[B_{NL}]$ is given as:

$$[B_{NL}] = [A][G],$$

where [*A*] is a matrix of slopes and [*G*] is a matrix of shape function derivatives defined by the relations:

$$\{g\} = [G]\{U\},$$

where $\{g\}$ is defined for the present 3D formulation as :

$$\{g\} = \left[\frac{\partial u_1}{\partial x}\ \frac{\partial u_2}{\partial x}\ \frac{\partial u_3}{\partial x}\ \frac{\partial u_1}{\partial y}\ \frac{\partial u_2}{\partial y}\ \frac{\partial u_3}{\partial y}\ \frac{\partial u_1}{\partial z}\ \frac{\partial u_2}{\partial z}\ \frac{\partial u_3}{\partial z}\right]^T$$

Now, substituting from Eqs. (6) and (7) into Eq. (5), we obtain :

$$\sum_e \{\delta U\}_e^T \left[\int_{V_e} [B]^T\{\sigma\}\,dV + \int_{V_e} [N]^T \rho\{\ddot{u}\}\,dV\right]$$

$$- \sum_e \{\delta U\}_e^T \left[\int_{V_e} [N]^T\{b\}\,dV + \int_{S_e} [N_s]^T\{p\}\,dS\right]$$

$$- \{\delta U\}^T\{F_c\} = 0 \tag{8}$$

where $[B] = [B_L] + [B_{NL}]$ and

$$\{\sigma\} = [C]\{\varepsilon\} = [C]\,[\bar{B}]\{U\}. \tag{9}$$

In Eq. (9), [*C*] is the material property matrix relating the strains to the stresses in global coordinate system.

Eq. (8) can be rewritten over the assemblage of all elements after dropping $\{\delta U\}$ from each term as follows :

$$\int_V [B]^T\{\sigma\}\,dV + \int_V [N]^T \rho\{\ddot{u}\}\,dV - \{R\} = 0, \tag{10}$$

where $\{R\}$ is the applied load vector given by :

$$\{R\} = \int_V [N]^T\{b\}\,dV + \int_S [N_s]^T\{p\}\,dS + \{F_c\}.$$

The equation of equilibrium given by Eq. (10) can be written at time t_{n+1} in a non-linear sense as :

$$\{\Psi_{n+1}\} = \int_V [B]^T\{\sigma_{n+1}\}\,dV$$

$$+ \int_V [N]^T \rho_{n+1}\{\ddot{u}_{n+1}\}\,dV - \{R_{n+1}\}, \tag{11}$$

where $\{\Psi_{n+1}\}$ is residual or out-of-balance force vector at a particular solution iteration.

Here Newmark time integration method, which is an implicit integration scheme, is used to solve equilibrium equation. Using Newmark method with constant average acceleration ($\alpha = 0.5$ and $\beta = 0.25$), the nodal acceleration vectors $\{\ddot{U}_{n+1}\}$ can be expressed in terms of nodal displacements $\{U_{n+1}\}$ as follows:

$$\{\ddot{U}_{n+1}\} = \frac{1}{\beta(\Delta t)^2}\{U_{n+1}\} - \left(\frac{1}{\beta(\Delta t)^2}\{U_n\} + \frac{1}{\beta(\Delta t)}\{\dot{U}_n\} + \frac{1-2\beta}{2\beta}\{\ddot{U}_n\}\right) \tag{12}$$

Eq. (12) along with Eq. (6) can be put into Eq. (11) to form :

$$\{\Psi_{n+1}\} = \int_V [B]^T\{\sigma_{n+1}\}\,dV$$

$$+ \frac{1}{\beta(\Delta t)^2}\left(\int_V [N]^T \rho_{n+1}[N]\,dV\right)\{U_{n+1}\} - \{F^M_{n+1}\} - \{R_{n+1}\} \tag{13}$$

Putting Eq. (9) into Eq. (13), an effective static equilibrium equation can be written as :

$$\{\Psi_{n+1}\} = \left(\int_V [B]^T[C][\bar{B}]\,dV + \frac{1}{\beta(\Delta t)^2}\left(\int_V [N]^T \rho_{n+1}[N]\,dV\right)\right)$$

$$\{U_{n+1}\} - \{F^{M}_{n+1}\} - \{R_{n+1}\} \tag{14}$$

In Eq. (13) and (14), $\{F^{M}_{n+1}\}$ can be referred to as the load vector due to inertia term at time t_{n+1} and is given as :

$$\{F^{M}_{n+1}\} = [M]\left(\frac{1}{\beta(\Delta t)^2}\{U_n\} + \frac{1}{\beta(\Delta t)}\{\dot{U}_n\} + \frac{1-2\beta}{2\beta}\{\ddot{U}_n\}\right) \tag{15}$$

In Eq. (15), $[M] = \int_V [N]^T \rho_{n+1} [N]\, dV$ is the mass matrix.

The solution of above non-linear Eq. (14) is achieved iteratively. Since Newton-Raphson incremental iterative scheme is adopted here, it is necessary to find relation between $\{d\Psi_{n+1}\}$ and $\{d U_{n+1}\}$.

Taking variation of residual force (Eq. (13)) with respect to $\{U_{n+1}\}$, we have:

$$\delta\{\Psi_{n+1}\} = \int_V [B]^T \delta\{\sigma_{n+1}\}\, dV + \int_V \delta[B]^T \{\sigma_{n+1}\}\, dV$$

$$+ \frac{1}{\beta(\Delta t)^2}\left(\int_V [N]^T \rho_{n+1} [N]\, dV\right)\delta\{U_{n+1}\} - \delta\{R_{n+1}\} \tag{16}$$

From the definition of tangent stiffness matrix,

$$\left[K^{T}_{n+1}\right]\delta\{U_{n+1}\} = \delta\{\Psi_{n+1}\} \tag{17}$$

where

$$\left[K^{T}_{n+1}\right] = \int_V [B]^T [C][B]\, dV + \int_V [G]^T \left[S_{n+1}\right][G]\, dV$$

$$+ \frac{1}{\beta(\Delta t)^2}\left(\int_V [N]^T \rho_{n+1} [N]\, dV\right) - \frac{\delta\{R_{n+1}\}}{\delta\{U_{n+1}\}} \tag{18}$$

In Eq. (18), [S] is a matrix of stress array and is given as :

$$[S] = \begin{bmatrix} \sigma_x [I] & \tau_{xy}[I] & \tau_{xz}[I] \\ & \sigma_y [I] & \tau_{yz}[I] \\ sym. & & \sigma_z [I] \end{bmatrix}$$

where $[I]$ is an identity matrix of size 3 x 3 for the present element considered. The system of simultaneous algebraic equations given in Eq. (17) is solved by frontal method during each iteration after imposing appropriate constraint conditions at the laminate boundaries.

Element Characteristics

In the present analysis, three-dimensional eight-noded isoparametric layered brick element (Fig.1) is developed to model the laminated structure. Layered version of element is different from the isotropic brick element in the sense that it accounts for changes in material properties and orientation of the plies inside the element. Element tangent stiffness matrix for this element is given as:

$$\left[K^{T}_{n+1}\right] = \int_{-1}^{+1}\int_{-1}^{+1}\int_{-1}^{+1} [B]^T [T]^T [\bar{C}][T][B] \det[J]\, d\xi\, d\eta\, d\zeta$$

$$+ \int_{-1}^{+1}\int_{-1}^{+1}\int_{-1}^{+1} [G]^T [S_{n+1}][G] \det[J]\, d\xi\, d\eta\, d\zeta$$

$$+ \frac{1}{\beta(\Delta t)^2}\left(\int_{-1}^{+1}\int_{-1}^{+1}\int_{-1}^{+1} [N]^T \rho_{n+1} [N] \det[J]\, d\xi\, d\eta\, d\zeta\right) - \frac{\delta\{R_{n+1}\}}{\delta\{U_{n+1}\}} \tag{19}$$

In the above equation, $[\bar{C}]$ is the material property matrix relating the strains within the ply to the stresses in ply coordinate system and $[T]$is the transformation matrix relating the strains in the ply principal directions to those in the global reference axis. The material density ρ, the elasticity matrix $[\bar{C}]$, transformation matrix $[T]$ and $[S]$ matrix in the above equation depend on the material properties and the orientations of the plies through the thickness of the element. When the material properties and ply orientations are same through the thickness, numerical integrations of the equation using Gaussian quadrature can be carried out at element level, otherwise it is accomplished from one ply-group to another ply-group through the element thickness. The stiffness matrix as given by Eq.(19) is of size 33 x 33 and includes coefficients pertaining to incompatible modes. However, these terms are eliminated by using the static condensation procedure and the condensed stiffness matrix is of the order 24 x 24 pertaining to the nodal degrees of freedom.

Calculation of Impact Force

When a composite laminate is impacted by a mass, local plastic deformation takes place in the contact region. This local deformation must be taken into account in order to predict contact force history accurately. Although the present formulation can simulate any type of complex contact conditions between impactor and laminate, the

modified version of Hertzian contact law proposed by Yang and Sun [17] based on static indentation tests for flat laminate and cylindrical shell is used in this study. This approach consists of determining the relationship between contact force F^c with the indentation depth α. Since the contact area is generally small in comparison with the dimensions of the laminate, a point load representing the resultant contact force is assumed.

The contact force F^c_{n+1} can be written in general form of contact law as:

$$F^c_{n+1} = \phi(\alpha_{n+1}) = \phi(d_{n+1} - w_{n+1})$$

$$= \phi\left(d_n + \dot{d}_n \Delta t - \frac{1}{4}\frac{F^c_n + F^c_{n+1}}{m}(\Delta t)^2 - w_{n+1}\right) \quad (20)$$

where d_{n+1} is the displacement of the centre point of the impactor at $(n+1)$ th time-step and calculated by applying Newmark's method to equation of motion of impactor as above. w_{n+1} is the displacement of mid-surface of the laminate at the impact point in the direction of impact. The last term in Eq.(19) consists of $\frac{dF^c_{n+1}}{dw_{n+1}}$, which can be found by differentiating Eq. (20).

Prediction of Impact Damage

It is reported in previous study [18] that intraply matrix cracking is the initial damage mode. Delamination (inter-ply cracking) initiates once the matrix crack reaches at the interfaces between the ply groups containing different fibre orientations after propagating throughout the thickness of the ply group that contained the cracked ply. This type of matrix crack is referred to as the "critical matrix crack". Accordingly, two failure criteria, critical matrix cracking criterion and delamination criterion are used.

Critical Matrix Cracking Criterion

In this study, three-dimensional matrix failure criterion originally proposed by Hashin [19] is used. This point stress criterion was modified by Choi and Chang [18] to be based on average stress through the thickness of a ply group, for predicting the critical matrix cracking. Based on major stresses attributing to transverse matrix cracking, the criterion for *n*th ply is given as:

$$\left(\frac{{}^n\bar{\sigma}_y}{n_Y}\right)^2 + \left(\frac{{}^n\bar{\tau}_{yz}}{n_{S_i}}\right)^2 = e_m^2 \begin{cases} Y = Y_t, & \text{if } \bar{\sigma}_y \geq 0; \\ Y = Y_c, & \text{if } \bar{\sigma}_y < 0. \end{cases} \quad (21)$$

where x-y-z is right-handed ply coordinate system with x-axis representing the fibre direction. Y_t and Y_c are the *in situ* ply transverse tensile and compressive strengths respectively within the laminate and S_i is the *in situ* interlaminar shear strength. ${}^n\bar{\sigma}_y$ and ${}^n\bar{\tau}_y$ are the averaged inplane transverse normal stress and averaged interlaminar transverse shear stress respectively within the *n*th ply. e_m is the strength ratio pertaining to matrix cracking. The region where e_m is greater than or equal to unity represents the location of the critical matrix cracking.

Delamination Criterion

Accurate simulation of delamination propagation is very difficult and complicated, since this phenomenon involves multiple dynamic crack propagation and interaction of delamination surfaces. To simplify the analysis, a semi-empirical criterion proposed by Choi and Chang [18] based on major stresses contributing to delamination formation is used to estimate the extent of delamination in composite. The criterion for nth interface is:

$$D_a\left[\left(\frac{{}^{n+1}\bar{\sigma}_y}{{}^{n+1}Y}\right)^2 + \left(\frac{{}^n\bar{\tau}_{yz}}{n_{S_i}}\right)^2 + \left(\frac{{}^{n+1}\bar{\tau}_{xz}}{{}^{n+1}S_i}\right)^2\right] = e_d^2 \begin{cases} Y = Y_t, & \text{if } \bar{\sigma}_y \geq 0; \\ Y = Y_c, & \text{if } \bar{\sigma}_y < 0. \end{cases} \quad (22)$$

Where D_a is an empirical constant, the value of which was suggested in [18]. The subscript *n* and *n+1* correspond to the upper and lower plies of the *n*th interface respectively. ${}^{n+1}\bar{\tau}_y$ is the averaged interlaminar longitudinal shear stress within the $(n+1)$th ply. e_d is the strength ratio pertaining to delamination. The region, where e_d is greater than or equal to unity at the end of the impact, gives the estimation of the delamination size.

Numerical Results and Discussions

The above non-linear finite element formulation was implemented in a specially developed computer code 'FACS' [20, 21]. A detail about the implementation and features of the code can be found using the hyperlink [21]. The model and the code is first validated using some

existing numerical solutions available in literature as discussed below.

Having validated the present approach, several example problems of T300/976 graphite/epoxy laminated cylindrical shells have been considered to study the impact behaviour of curved composite laminate undergoing large deformation. The problem descriptions of impact on a general doubly curved shell are depicted in Fig.2 in which $x_1 - x_2 - x_3$ is the right-handed global (reference) coordinate system and impacted side is the first layer in the stacking sequence. For all the example problems considered, the mesh size chosen is 16 x 16 x 4 elements and mesh density is kept higher at the centre than the sides in the curvilinear plane of the laminate.

Benchmark Results

Large Deformation of Hinged-hinged and Pinned-pinned Beams

As an example, a benchmark problem of a simply-supported isotropic beam involving geometric nonlinearity as solved by Reddy [22] is considered. A uniform beam of length L=100, cross-section dimensions of 1 x 1, made of a material with $E = 30 \times 10^6$ is simply supported at both ends and subjected to a uniformly distributed load of intensity q per unit length. The units are consistently chosen, so that the exact deflection at the middle of the beam in linear bending theory is 0.5208, when $q = 1$. In linear bending theory, where the beam is assumed to undergo pure bending (i.e. there is no axial deformation); it is immaterial to consider whether the beam is allowed free movement in the axial direction at the supported ends. However, in non-bending, this is a crucial distinction. Hinged-hinged (HH) condition is designated for the case where there is no axial restraint at both ends and pinned-pinned (PP) condition for the one where there is full restraint. In the former case, inextensional bending occurs which is largely of a linear nature, and in the latter case, bending with extension exists. Both the cases are considered here. Using symmetry, half of the beam is modeled with 8 x 1 x 1 elements.

The HH case is ideal to test the consistency aspect of the problem. As a non-linear element formulation is being used, a correct model should be able to recover the purely linear bending response under increasing load. This is possible only if the element can ensure that the inextensional axial condition (i.e. there is no axial restraint at both ends, no axial force should develop) is consistently recovered throughout. The PP case is ideal to examine the significance of the consistency aspect of the problem where the non-linear action becomes important. Table-1 shows the deflection under the load as q increases from 1 to 10. Results from Reddy [22] are also shown in which two versions of beam element has been used. The first version which will have locking uses 2 points integration for bending energy and extensional energy while the second version which will be lock free uses 2 points integra-

Table-1 : Central Deflection for a Simply Supported Beam Under Uniformly Distributed Load (UDL)

UDL per Unit Length, q	Present Solution	Reference [22]	
	2 x 2 x Integration Rule	2 x 2 Selective (Energy Based) Integration Rule	2 x 1 Selective (Energy Based) Integration Rule
(A) Hinged-Hinged (HH) Condition			
1	0.517697	0.5108	0.5208
2	1.03519	0.9739	1.0417
3	1.55206	1.3764	1.5625
4	2.06791	1.7265	2.0833
5	2.58231	2.0351	2.6042
6	3.09489	2.3116	3.1250
7	3.60521	2.5630	3.6458
8	4.11301	2.7930	4.1667
9	4.61784	3.0060	4.6875
10	5.11938	3.2051	5.2083
(B) Pinned-Pinned (PP) Condition			
1	0.367949	0.3669	0.3687
2	0.545474	0.5424	0.5466
3	0.664471	0.6601	0.6663
4	0.756362	0.7510	0.7591
5	0.832352	0.8263	0.8361
6	0.897760	0.8912	0.9027
7	0.955557	0.9485	0.9617
8	1.00758	1.0002	1.0150
9	1.05506	1.0473	1.0638
10	1.09885	1.0908	1.1089

tion for bending energy and 1 point integration for the extensional energy. It is clear from the Table that the present element model is able to capture both the behavior correctly.

Clamped 16-ply Symmetric Laminate Subjected to Uniform Load

Next a 16-ply $\left[\pm 45/0_2^0/\mp 45^o/90_2^0\right]_S$ graphite-epoxy square laminate of size b = 254 mm and thickness h = 2.114 mm is considered as investigated by Noor [23]. The plate is clamped on all edges and subject to uniform load q. The material properties of graphite-epoxy unidirectional ply are taken as:

$E_x = 131$ GPa ; $E_y = E_z = 13.03$ GPa ; $G_{xy} = G_{yz} = G_{xz} = 6.41$ GPa ; $\nu_{xy} = \nu_{yz} = \nu_{xz} = 0.38$.

Figure 3 gives the comparison between present analysis and the results by Noor [23] for laminate central deflection of the mid-ply. A good agreement can be observed.

Clamped [0/90] Asymmetric Cross-ply Cylindrical shell Panel Subjected to Uniform Load

The asymmetric cross-ply cylindrical shell panel studied by Reddy and Chandrashekhara [24] is investigated. The radius and length of the cylindrical shell panel are 64.5 m and 12.9 m respectively. The angle subtended by the arc is 0.2 radian. The thickness of the shell is 64.5 mm. The material properties used are same as those of [24]:

$E_x = 172$ GPa ; $E_y = E_z = 7$ GPa ; $G_{xy} = G_{yz} = G_{xz} = 3.5$ GPa ; $\nu_{xy} = \nu_{yz} = \nu_{xz} = 0.25$.

The load-deflection curve of the non-linear solution is given in Fig.4 along with the results of reference [24]. Fairly good agreement is seen.

Impact Response of a Rectangular Graphite/epoxy Laminated Plate

As another example, impact on a rectangular graphite/epoxy laminated plate with a ply orientation of $[0/-45/45/90]_{2S}$ is investigated with plate dimensions and impactor parameters to be same as that taken by Kumar et al. [25]. A non-linear analysis was carried out for this problem. The results of contact force and plate centre displacement are presented in Fig. 5 along with the results of linear analysis reported in [25]. There is only a negligible difference between linear and non-linear solutions for this particular problem which indicates that the non-linearity effect is not much pronounced for the case where maximum plate deflection is of the order less than the plate thickness.

Impact Response

T300/976 Graphite/epoxy cylindrical shells of different dimensions and curvatures with two different lay-ups $[90_4/0_8/90_4]$ and $[45_4/-45_8/45_4]$ and clamped on their edges are considered. At first, $[90_4/0_8/90_4]$ cylindrical shell is taken with geometric properties: $a = b = 100$ mm; $R_1 = R =$ a, 10a; and $R_2 = \infty$ (Fig. 2). The impactor is a steel mass of 200 gm having a half sphere head of 10 mm diameter and initial velocity 5 ms^{-1}. The material properties of fiberite T300/976 graphite/epoxy composite are considered as listed elsewhere [18]. The time step Δt is chosen to be 8 μs. The results of contact force, impactor displacement and shell centre displacement are presented in Fig. 6 for linear analysis of shell curvature R = 10a and both linear and non-linear analyses of shell curvature R = a. An increase in contact period and reduction in peak contact force resulted in using a non-linear analysis when compared with using a linear analysis. This indicates that the overall stiffness of the laminate decreased when geometrical non-linearity is incorporated in the solution. Although, there is no substantial difference in maximum central deflection in the two analyses for this particular problem, post-contact amplitude of free vibration is considerably less in non-linear case. Effect of shell curvature is also shown in the figure. The maximum contact force increases and both contact duration and amplitude of shell response decrease with decrease in shell radius. This signifies that increasing the curvature has a stiffening effect on the cylindrical shell.

Next, cylindrical shell of larger dimensions $a = b = 300$ mm and curvature R = a is considered which is again clamped on its edges and is subjected to impact by a steel mass of 200 gm having a half sphere head of 10 mm diameter and initial velocity 10 ms^{-1}. The results are plotted in Fig.7 for linear and non-linear solutions of $[90_4/0_8/90_4]$ layup and non-linear solution of $[45_4/-45_8/45_4]$ layup. Again an increase in contact duration and reduction in maximum contact force are observed in case of non-linear approach. Maximum central deflection also increased considerably in non-linear solution. A comparison of this result with results of Fig.6 depicts that effect of geometrical non-linearity obviously increased with in-

crease in maximum shell deflection. Non-linear solutions of the two different lay-ups depict that $[90_4/0_8/90_4]$ cross-ply laminate produces a higher maximum contact force combined with higher contact duration and higher shell centre deflection in comparison to $[45_4/-45_8/45_4]$ angle-ply laminate.

Impact-induced Damages

Impact-induced damages (critical matrix cracking and the extent of delamination) are studied for the above cylindrical shells with two different lay-ups $[90_4/0_8/90_4]$ and $[45_4/-45_8/45_4]$. The shell with $[90_4/0_8/90_4]$ lay-up with dimensions $a = b = 100$ mm and curvatures $R = 10a$ and $R = a$ is subjected to impact by a steel mass of 200 gm and nose radius 5 mm traveling at a velocity of 5 ms^{-1}. Critical matrix cracking takes place in the bottom $[90_4]$ ply group for all the cases. The value of strength ratio, e_m at any point in the shell is found to be maximum at time approximately 768 μs for $R/a = 10$ (linear analysis), at 536 μs for $R/a = 1$ (linear analysis) and at 592 μs for $R/a = 1$ (non-linear analysis), as plotted in isometric view in Fig. 8. The critical matrix cracking failure contour is extended much wider along the fibre direction of the cracked $[90_4]$ ply group than in the direction normal to the fibre direction.

The maximum values of strength ratio, e_d (impact-induced delamination criterion) in the bottom 0/90 plies interface during the impact are plotted in Fig.9 for the three cases. It is seen that delamination propagated much wider in the fibre direction of the $[90_4]$ ply group below the delaminated interface than in the direction normal to it and approached a peanut shape.

From Figs.8 and 9, it can be observed that there is a considerable increase in the sizes of both the damages when non-linearity is considered in the solution. A small increase in damage sizes is also seen with increase in shell curvature. Maximum strength ratio, e_m occurred earlier in case of higher curvature mainly because contact duration is less in this case.

Impact-induced damages are also predicted for the example problem of Fig.7. The value of strength ratio, e_m at any point in the shell with $[90_4/0_8/90_4]$ lay-up happened to be maximum in the bottom $[90_4]$ ply group at time approximately 1020 μs in case of linear analysis and 1128 μs in case of non-linear analysis. For the non-linear solution of $[45_4/-45_8/45_4]$ lay-up, the value of strength ratio, e_m at any point in the bottom $[45_4]$ ply was predicted to be maximum at time approximately 852 μs. The results are plotted in Fig.10. The maximum value of strength ratio, e_d and predicted delamination size in the bottom 0/90 plies interface of $[90_4/0_8/90_4]$ lay-up and in the bottom -45/45 plies interface of $[45_4/-45_8/45_4]$ lay-up after the impact are plotted in Fig.11. Again there is a considerable increase in size of damages in case of non-linear solution. A different representation of impact damage results for $[45_4/-45_8/45_4]$ lay-up is shown in Fig.12 for the sake of clarity. It is seen again that there is a clear alignment of both the damages in the direction of fibre in the lowermost $[45_4]$ ply group of $[45_4/-45_8/45_4]$ lay-up. The profiles of strength ratios, e_m and e_d are also noticeably different for the two different lay-ups.

Summary

Three-dimensional non-linear finite element and transient dynamic analysis of laminated composite cylindrical shells subjected to transverse impact is performed and implemented by a specially developed computer code. A layered version of isoparametric eight-noded hexahedral element with incompatible modes is developed which incorporates geometrical non-linearity based on total Langragian approach. The tangent stiffness matrix accounting for the geometric non-linearity is formulated using generalized Greens strain tensor. The non-linear system of equations was solved iteratively using Newton-Raphson method by considering a suitable displacement and force convergence norms. Several numerical examples of graphite/epoxy laminated cylindrical shells are considered and parametric studies were performed. Non-linear geometrical effects on impact response and resulting damages are studied for problem configurations with different cases of impactor velocity, shell dimension, shell curvature and fibre orientation of plies. Although the solution parameters such as mesh density and time step selected here were found to provide stable solutions for the problem cases considered, it is expected that more quantitative inferences will result with increasing mesh density and decreasing analysis time step.

Some important observations were deduced from the study. When geometrical non-linearity was considered in the analysis, a reduction in peak contact force resulted in combination with an increase in both contact period and maximum shell deflection. The difference in impact response is found to be more significant for the cases when the maximum shell deflection is higher than the shell thickness. Considerable changes in the size and profile of

both the impact damages (critical matrix cracking and delamination) are also noticed as a result of using non-linear approach.

References

1. Cantwell, W. J. and Morton, J., "The Impact Resistance of Composite Materials - A Review", Composites, Vol. 22, pp. 347-362, 1991.

2. Abrate, S., "Impact on Laminated Composites: Recent Advances". Applied Mechanics Review, Vol. 47, pp. 517-544, 1994.

3. Aggour, H. and Sun, C.T., "Finite Element Analysis of a Laminated Composite Plate Subjected to Circularly Distributed Central Impact Loading", Computers and Structures, Vol. 28, pp. 729-736, 1988.

4. Wu, H. T. and Springer, G. S., "Impact Induced Stresses, Strains, and Delaminations in Composite Plates", Journal of Composite Materials, Vol. 22, pp. 533-560, 1988.

5. Wu, H.T. and Chang, F.K., "Transient Dynamic Analysis of Laminated Composite Plates Subjected to Transverse Impact", Computers and Structures, Vol. 31, pp. 453-466, 1989.

6. Nosier, A., Kapania, R.K. and Reddy, J.N., "Low Velocity Impact of Laminated Composites Using a Layerwise Theory", Computational Mechanics, Vol.13, pp. 360-379, 1994.

7. Kim, S.J., Goo, N.S. and Kim, T.W., "The Effect of Curvature on the Dynamic Response and Impact Induced Damage in Composite Laminates", Composite Science and Technology, Vol.57, pp. 763-773, 1997.

8. Ambur, D.R., Starnes, J.H. Jr. and Prasad, C.B., "Low-Speed Impact Damage Initiation Characteristics of Selected Laminate Composite Plate", AIAA Journal, Vol. 33, pp. 1919-1925, 1995.

9. Chandrashekhara, K. and Schroeder, T., "Nonlinear Impact Analysis of Laminated Cylindrical and Doubly Curved Shells", Journal of Composite Materials, Vol. 29, pp. 2160-2179, 1995.

10. Kam, T.Y., Sher H.F. and Chao, T.N., "Prediction of Deflection and First-Ply Failure Load of Thin Laminated Composite Plates via the Finite Element Approach", International Journal for Solids and Structures, Vol. 33, pp. 375-398, 1996.

11. Ganapathy, S. and Rao K.P., "Failure Analysis of Laminated Composite Cylindrical/Spherical Shell Panels Subjected to Low-Velocity Impact", Computers and Structures, Vol. 68, pp. 627-641, 1998.

12. Krishnamurthy, K.S., Mahajan, P. and Mittal, R.K., "A Parametric Study of The Impact Response and Damage of Laminated Cylindrical Composite Shells", Composite Science and Technology, Vol. 61, pp. 1655-1669, 2001.

13. Zhu, L., Chattopadhyay, A. and GoldBerg, R.K., "Multiscale Analysis Including Strain Rate Dependency for Transient Response of Composite Laminated Shells", Journal of Reinforced Plastics and Composites, Vol. 25, pp. 1795-1831, 2006.

14. Kumar, S., "Analysis of Impact Response And Damage in Laminated Composite Shell Involving Large Deformation and Material Degradation", Journal of Mechanics of Materials and Structures, Vol.3, pp.1741-1756, 2008.

15. Sanders, Jr. J.L., "An Improved First Approximation Theory for Thin Shells", NASA Report R-24, 1959.

16. Stein, M., "Nonlinear Theory for Plates and Shells Including the Effects of Transverse Shearing", AIAA Journal, Vol. 24, pp. 1538-1544, 1986.

17. Yang, S.H. and Sun, C.T., "Indentation Law for Composite Laminates", ASTM STP 787, pp. 425-449, 1982.

18. Choi, H.Y. and Chang, F.K., "A Model for Predicting Damage in Graphite/Epoxy Laminated Composites from Low-Velocity Point Impac"t, Journal of Composite Materials, Vol. 26, pp. 2134-2169, 1992.

19. Hashin, Z., "Failure Criteria for Unidirectional Fibre Composites". Journal of Applied Mechanics, Vol.47, pp. 329-334, 1980.

20. Kumar, S., "Finite Element Analysis of Impact-Induced Deformations, Stresses and Damages in Composite Laminates", Ph.D. Thesis, Indian Institute of Technology, Kharagpur, 1998.

21. Finite Element Analysis Software 'FACS', URL: http://www.facssoft.com.

22. Reddy, J.N., "An Introduction to Non-Linear Finite Element Analysis", Oxford University Press, Oxford, 2004.

23. Noor, A.K., "Hybrid Analytical Technique for Nonlinear Analysis of Structures", AIAA Journal, Vol.23, pp. 938-946, 1985.

24. Reddy, J.N. and Chandrashekhara, K., "Nonlinear Analysis of Laminated Shells Including Transverse Shear Strains", AIAA Journal, Vol. 23, pp. 440-441, 1985.

25. Kumar, S., Rao, B.N. and Pradhan B., "Effect of Impactor Parameters and Laminate Characteristics on Impact Response and Damage in Curved Composite Laminates", Journal of Reinforced Plastics and Composites, Vol. 26, pp. 1273-1290, 2007.

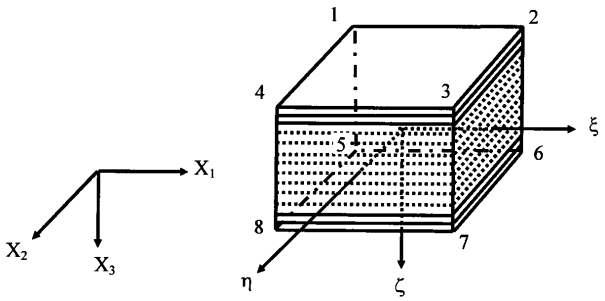

Fig.1 Layered Version of Eight-noded Isoparametric Brick Element

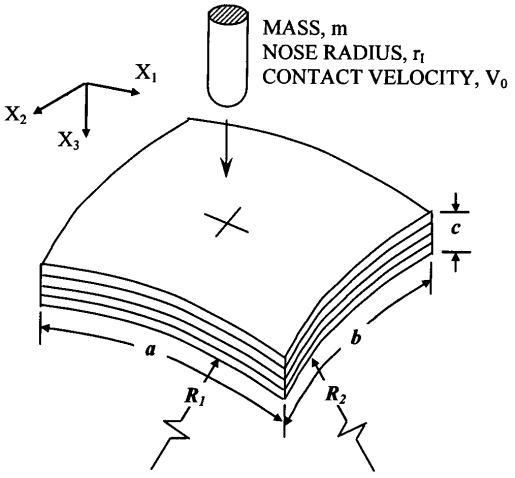

Fig.2 Problem Description of Impact on a General Doubly Curved Shell

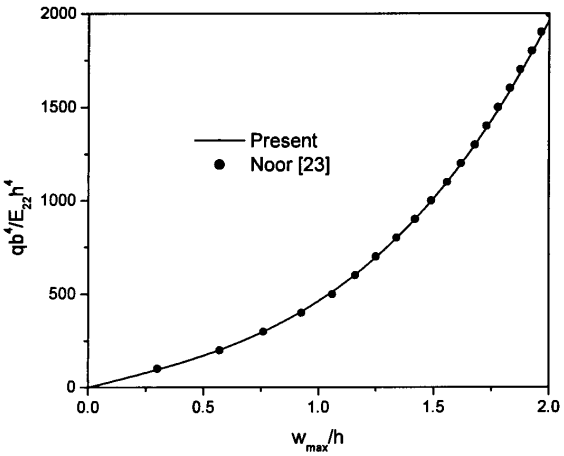

Fig.3 Load-deflection Curve for 16-ply $\left[\pm 45/0_2^o/\mp 45^o/90_2^o\right]_S$ *Square Laminate (Size b = 254 mm and thickness h = 2.114 mm) with Clamped Edges and Subjected to Uniform Load*

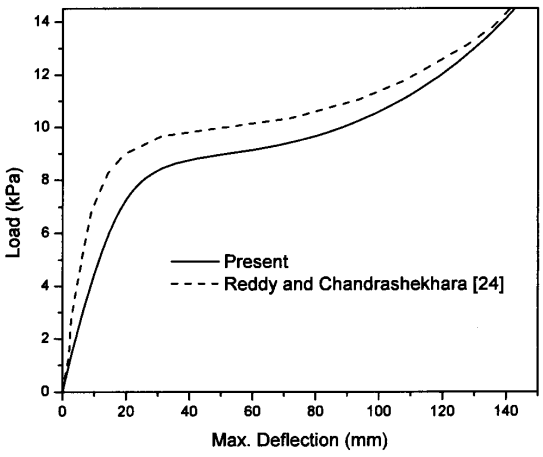

Fig.4 Load-Deflection Curve for Clamped [0/90] Asymmetric Cross-ply Cylindrical Shell Panel Subjected to Uniform Load

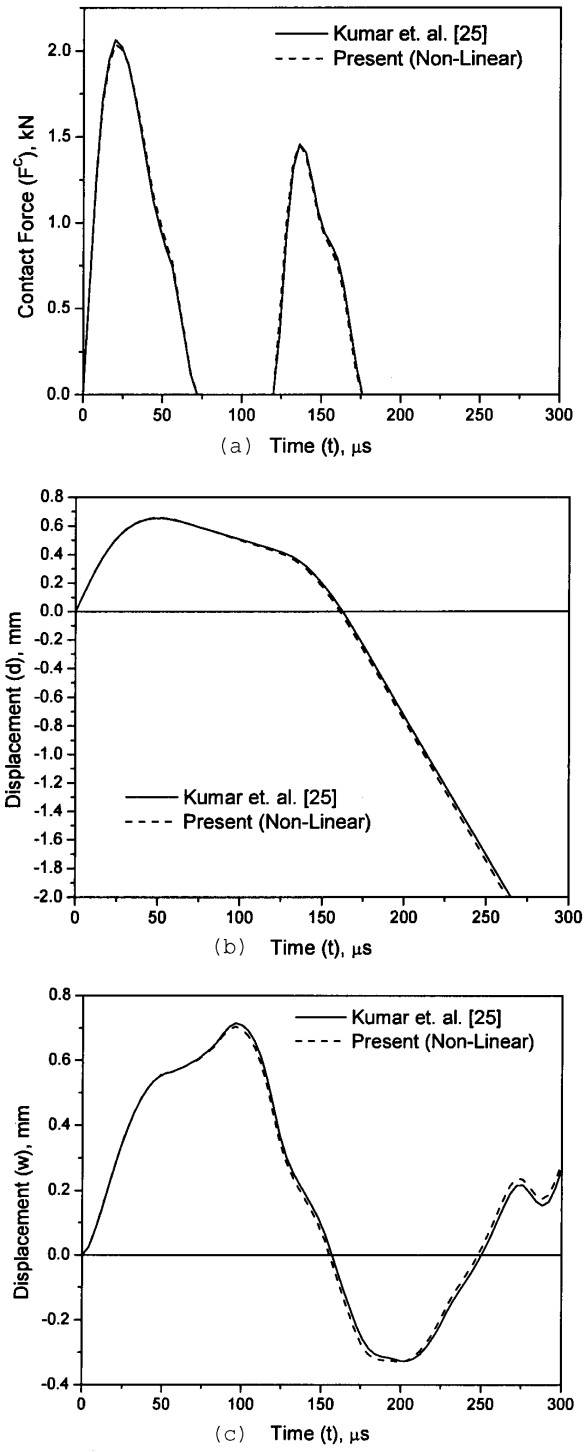

Fig.5 Comparison of (a) Contact force, (b) Impactor displacement and (c) plate centre displacement in a 76.2 by 76.2 mm T300/934 graphite/epoxy laminated plate ($[0/45/45/90]_{2S}$) with clamped edges impacted by 12.7 mm diameter aluminum sphere at a velocity of 25.4 ms^{-1}.(time step, Δt = 4 μs)

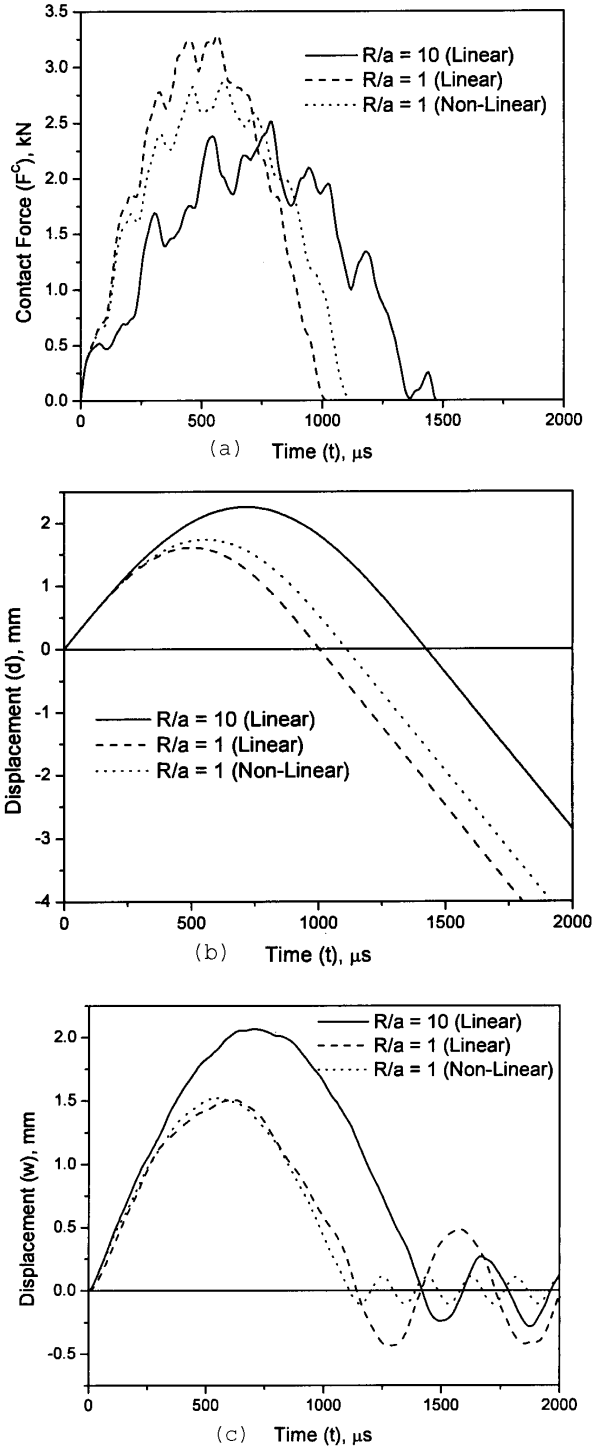

Fig.6 (a) Contact force, (b) Impactor displacement and (c) Centre displacement in graphite/epoxy cylindrical shells ($[90_4/0_8/90_4]$) (a = b = 100 mm; R = 10a and R = a), with clamped edges impacted by blunt-ended steel cylinder of nose radius 5mm and mass 200 gm having initial velocity of 5 ms^{-1}.(time step, Δt = 8 μs)

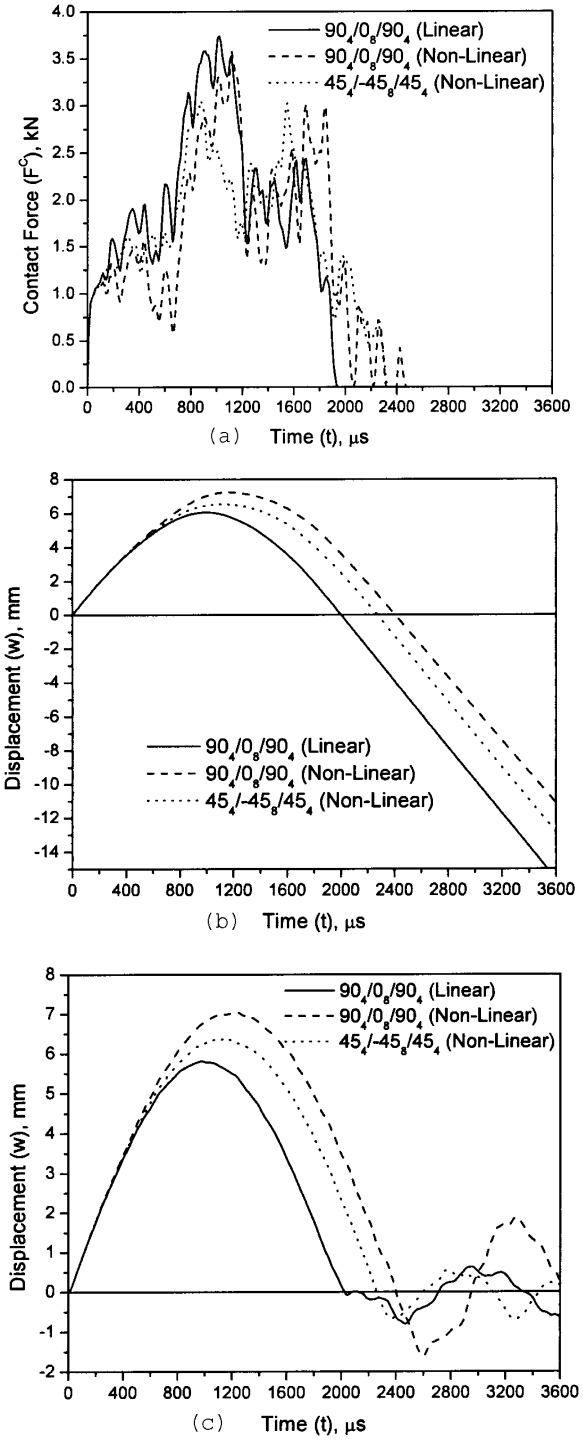

Fig.7 (a) Contact force, (b) Impactor displacement and (c) Centre displacement in graphite/epoxy cylindrical shells ([$90_4/0_8/90_4$] and [$45_4/-45_8/45_4$] layups) (a = b = 300 mm; R = a), with clamped edges and impacted by blunt-ended steel cylinder of nose radius 5mm and mass 200 gm having initial velocity of 10 ms^{-1} (time step, Δt = 8 μs)

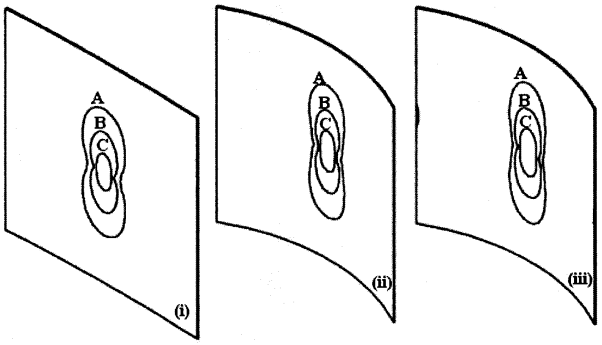

Fig.8 Maximum strength ratio, e_m in bottom [90_4] ply of [$90_4/0_8/90_4$] cylindrical shells (dimensions : a = b = 100 mm) having different curvatures (i) R/a = 10 (linear analysis), (ii) R/a = 1 (linear Analysis) and (iii) R/a = 1 (non-linear analysis), all with clamped edges and impacted by 200 gm mass at a velocity of 5 ms^{-1}.(e_m values : A = 0.2, B = 0.5, C = 1.0)

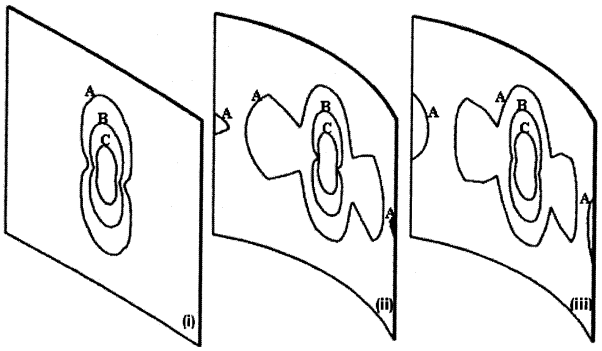

Fig.9 Maximum strength ratio, e_d and predicted delamination sizes at 0/90 interface of [$90_4/0_8/90_4$] cylindrical shells (dimensions : a = b = 100 mm) having different curvatures (i) R/a = 10 (linear analysis), (ii) R/a = 1 (linear Analysis) and (iii) R/a = 1 (non-linear analaysis), all with clamped edges and impacted by 200 gm mass at a velocity of 5 ms^{-1}. (e_d values : A = 0.2, B = 0.5, C = 1.0)

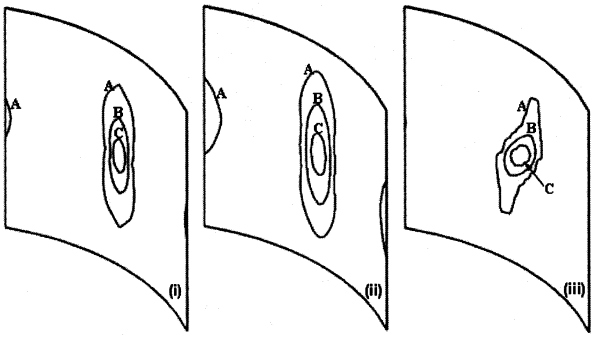

Fig.10 Maximum strength ratio, e_m in cylindrical shell (dimensions : a = b = 300 mm; R = a) with clamped edges and impacted by 200 gm mass at a velocity of 10 ms^{-1} : (i) in bottom [90_4] ply of [$90_4/0_8/90_4$] lay-up (linear analysis), (ii) in bottom [90_4] ply of [$90_4/0_8/90_4$] lay-up (non-linear analysis) and (iii) in bottom [45_4] ply of [$45_4/-45_8/45_4$] lay-up (non-linear analysis). (e_m values : A = 0.2, B = 0.5, C = 1.0)

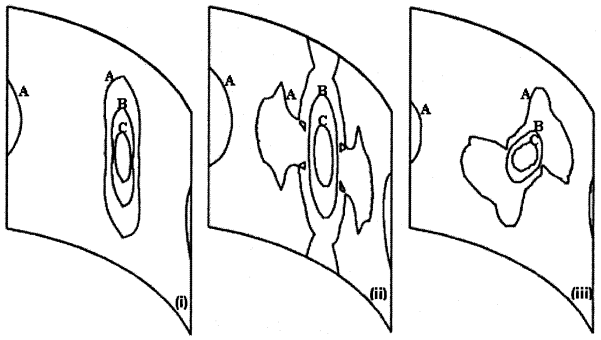

Fig.11 Maximum Strength Ratio, e_d and predicted delamination sizes in cylindrical shell (dimensions : a = b = 300 mm; R = a) with clamped edges and impacted by 200 gm mass at a velocity of 10 ms^{-1} : (i) at 0/90 interface of [$90_4/0_8/90_4$] lay-up (linear analysis), (ii) at 0/90 interface of [$90_4/0_8/90_4$] lay-up (non-linear analysis) and (iii) at -45/45 interface of [$45_4/-45_8/45_4$] lay-up (non-linear analysis). (e_d values : A = 0.2, B = 0.5, C = 1.0)

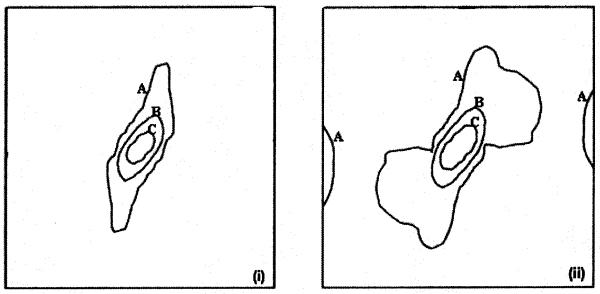

Fig.12 (i) Maximum strength ratio, e_m in bottom [45_4] ply and (ii) Maximum strength ratio, e_d at -45/45 interface in [$45_4/-45_8/45_4$] lay-up cylindrical shell (dimensions : a = b = 300 mm; R = a) with clamped edges and impacted by 200 gm mass at a velocity of 10 ms^{-1}. (Values : A = 0.2, B = 0.5, C = 1.0)